Chapter 5

Evaluation of Johnson-Cook parameters for plastic deformation of Fe-30Mn-9Al-0.8C low-density steel of fixed yield strength: simulation and its validation

5.1 Introduction

The SS1 steel finds extensive use in forged parts of automotive (A front-side member (energy absorption) and A-Pillar (anti-intrusion)), military (armor applications), and structural components (beams and columns) due to its high ductility and high toughness in a series of Fe-Mn-Al-C steels [169-170]. Both theoretical and experimental investigations are required for austenite based Fe-Mn-Al-C low-density steel in order to determine the flow stress during deformation. Since the forming of automobile parts occurs at intermediate strain rate level or above, the automobile industry needs a comprehensive understanding of strain rate-based deformation behaviour. Therefore, this present work aims at revealing the effect of strain, strain rate, and temperature on the deformation mechanism of Fe-Mn-Al-C light weight steel through series of tensile tests conducted at quasi-static, moderate strain rate and temperature conditions. Using experimental data, the characteristic parameters are determined to establish the empirical J-C model. The reliability of the J-C parameters has further been improved by using GA based optimization technique. Thereafter, using the improved J-C constitutive equation, numerical simulation (using ABAQUS explicit software) is performed for two different tensile tests where the simulation results are compared with the experimental curves.

5.2 Evaluation of J-C parameters

5.2.1 Tensile behaviour of solutionised and WQ Fe-30Mn-9Al-0.8C steel

The experimental tensile stress-strain curves of low-density steel are shown in Fig. 25 for various strain rates and temperatures. The yield strength and ultimate tensile strength have

been evaluated as 380 MPa and 762 MPa from the quasi-static tensile test performed at strain rate of 5 x 10^{-4} s^{-1}. From the tensile test curves, a rapid increase in flow stress is observed to a peak value in the plastic deformation zone which shows strain hardening ability of SS1 low-density steel at all strain rates and temperature conditions. Also, the steel possesses exceptionally high plastic elongation up to around 75 % which declines to around 60% when the strain rate is increased to 10^{-1} s^{-1}. While performing tensile test at elevated temperature, the elongation has slightly been increased at 150℃ and maximum elongation observed is at 300℃, then again it decreases at 450℃. Generally, the parameter that defines the strength and the formability of forged component is considered in term of product of tensile strength (TS) and total elongation (TE). The commercially used steels in automobile application like low carbon steel, TRIP steel, and TWIP steel have PSE value 15000 MPa%, 20000 MPa%, and 50000 MPa%, respectively [171], [172]. However, the PSE value for the present steel in the solutionized and WQ condition is greater than 57000 MPa%. Typically, the flow stress increases with increasing strain rate in austenite low-density steel confirming positive strain rate sensitivity [173-174] while some researchers confirm negative strain rate sensitivity in the strain rate range of 10^{-2}-10^{2} s^{-1} [175] .

From Fig. 25a, no significant difference is observed in the deformation characteristic of flow curve with increasing the strain rate. The yield strength is increased slightly with increase in strain rate while ultimate strength remains almost the same. The decrease in hardening rate at higher strain rate is due to ease in the dynamic recovery of dislocations. The dynamic recovery of dislocations is accelerated due to adiabatic heating at higher strain rate, which causes a negative effect on the strain hardening. Thereby, the strain hardening capability is weakened in the steel deformed at high strain rate [176]. Because of the increase of temperature during deformation from 25℃ to 450℃ as shown in Fig. 25b, there is decrease in yield strength and ultimate strength.

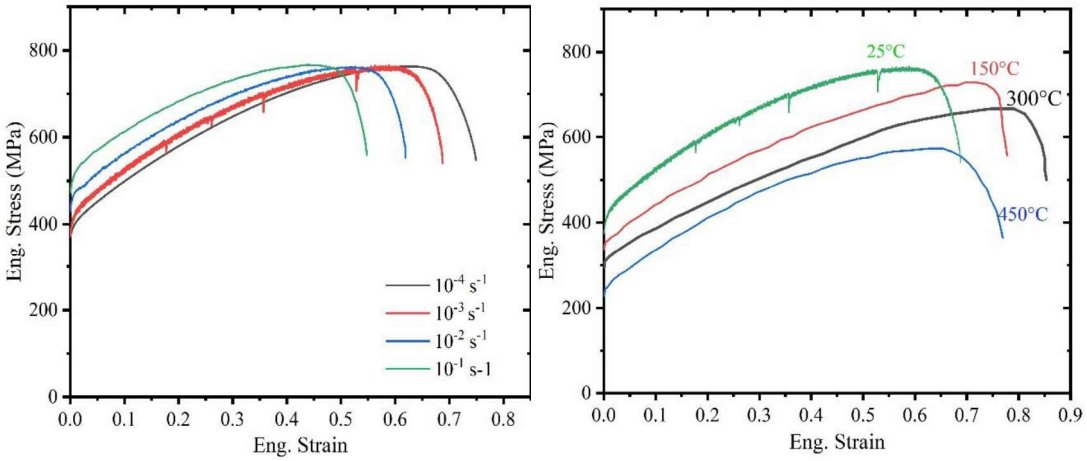

Fig. 25: Stress-strain curves obtained after tensile test performed at (a) different strain rates and (b) at different temperatures.

As reported by Yoo and Park [84], microband-induced plasticity, i.e. the main deformation mechanism of the austenitic low-density steel, results from planar glide. However, thermal energy increases the mobility of dislocations on their own glide plane overcoming obstacles such as short range ordering or clustering in the glide plane. Yoo et al. have reported similar behavior of strain hardening with strain rate and temperature for Fe-28Mn-9-Al-0.9C alloy steel [45].

5.2.2 Determination of J-C parameters using curve fitting.

When the effects of strain rate and temperature are neglected, i. e. at reference strain rate and reference temperature, the Eq. (10) reduces to:

$$\sigma_{eq} = (A + B\varepsilon^{n}) \tag{13}$$

Where, A is the yield strength of material at 0.002 strain level. Rearranging the above equation and taking natural logarithm on both sides, the Eq. (13) can be written as:

$$\ln(\sigma_{eq} - A) = n \ln \varepsilon + \ln B \tag{14}$$

The hardening parameters are determined by plotting the graph between $\ln(\sigma_{eq} - A)$ vs $\ln \varepsilon$ and fitting the data points using linear regression method as shown in Fig. 26. $\ln B$ is the intercept of fitted line and n is the slope.

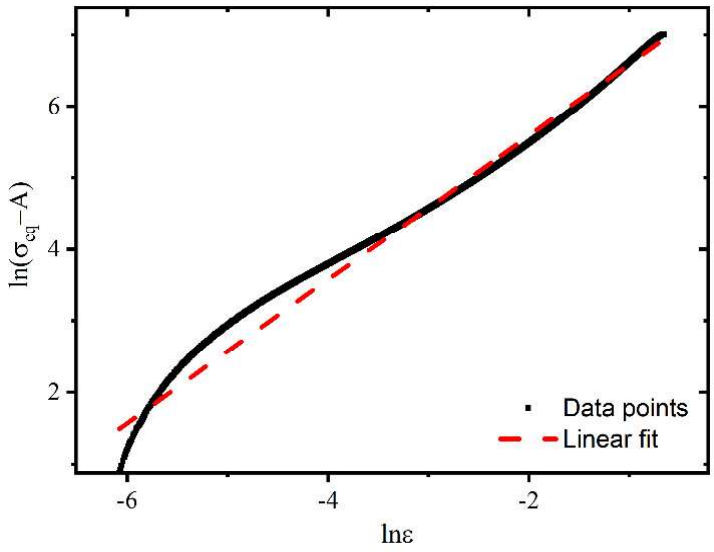

Fig. 26: Logarithmic relationship of stress-strain at reference conditions for finding B and n parameters.

Neglecting the thermal softening effect, the Eq. (10) can be remodeled for the stress-strain relationship at room temperature as:

$$\frac{\sigma_{eq}}{(A + B\varepsilon^n)} = 1 + Cln\left(\frac{\dot{\varepsilon}}{\dot{\varepsilon}_0}\right) \tag{15}$$

Substituting the stress-strain data at different strain rates and the values of A, B and n obtained as 380 MPa, 1860 MPa, and 1.02 respectively are put into Eq. (15) and then curves of $\frac{\sigma_{eq}}{(A+B\varepsilon^n)}$ vs $ln\left(\frac{\dot{\varepsilon}}{\dot{\varepsilon}_0}\right)$ have been plotted as shown in Fig. 27.

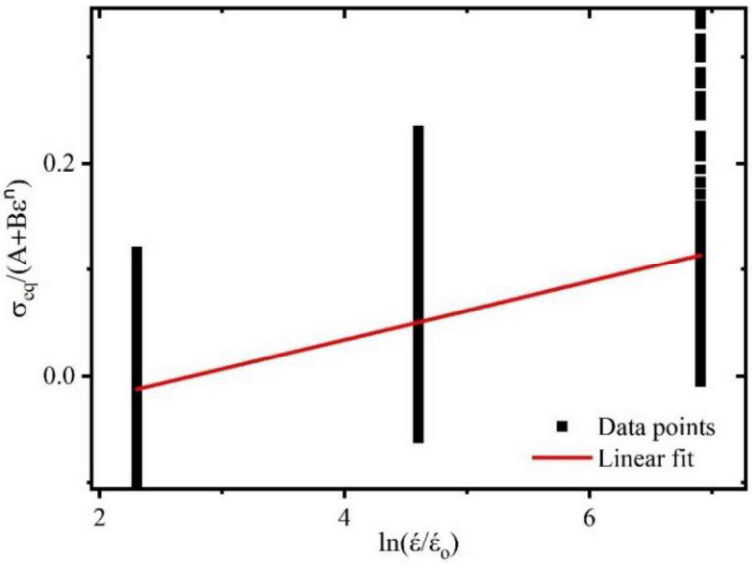

Fig. 27: Logarithmic relationship of stress-strain for finding C parameter.

Subsequently, linear fitting is carried out using the first-order regression model with an intercept value of 1 considering flow stress values at three different strain rates. The slope of the fitting curve gives the material strain rate parameter 'C' equal to 0.0067.

Neglecting the effect of strain rate, i.e. at reference strain rate, Eq. (10) can be modified as:

$$\sigma_{eq} = (A + B\varepsilon^n)\left[1 - \left(\frac{T - T_r}{T_m - T_r}\right)^m\right] \tag{16}$$

Rearranging and taking natural logarithm on both sides of Eq. (16) can be written as:

$$\ln\left(1 - \frac{\sigma_{eq}}{(A + B\varepsilon^n)}\right) = m \ln\left(\frac{T - T_r}{T_m - T_r}\right) \tag{17}$$

The curves between $\ln\left(1 - \frac{\sigma_{eq}}{(A+B\varepsilon^n)}\right)$ vs $\ln\left(\frac{T-T_r}{T_m-T_r}\right)$ have been plotted as shown in Fig. 28. The slope of the linear fitting curve gives the material constant 'm' and the value has been determined to be 0.64.

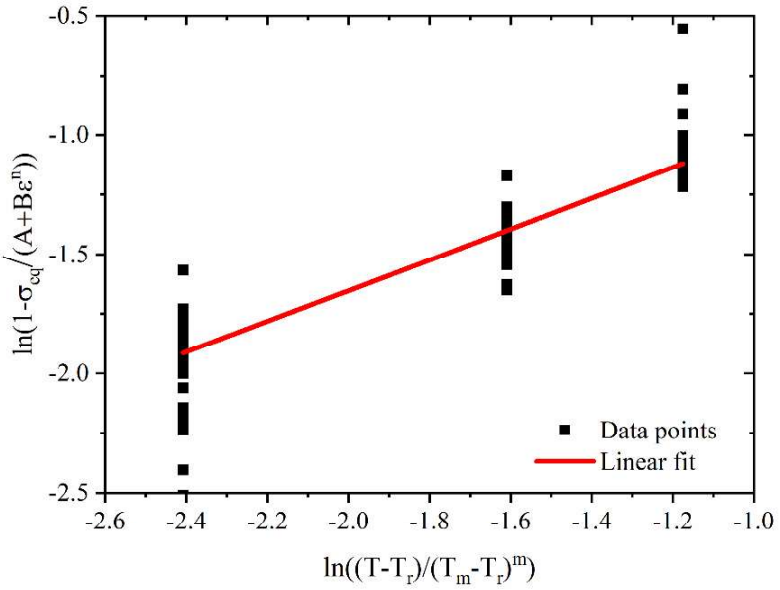

Fig. 28: Logarithmic relationship of stress-strain for finding *m* parameter.

5.2.3 Optimized J-C parameters by GA.

Using the true stress-strain data from tensile tests at different strain rates and temperatures, the difference between the experimental and calculated stress values are minimized by defining the objective function. Four different strain rates (10^{-4}, 10^{-3}, 10^{-2} and 10^{-1} s^{-1}) and four temperature levels (25℃, 150℃, 300℃ and 450℃) including refrence conditions are considered in objective functions. For the purpose of computing the calculated stress, J-C relation as given in Eq. (10) is used. The optimization of J-C parameters is performed in optimization toolbox equipped in MATLAB software and 43 sets of stress-strain data in plastic zone have been created by taking upper and lower bounds of B, n, C and m values. The optimal set of parameters from the GA toolbox such as population size, crossover fraction, function tolerance etc. were selected for the optimization analysis. Trial-and-error was used to specify the parameters' values in order to find the ones that yield the best results while not significantly lengthening computation time. The optimization procedure is terminated if the fitness function-related stopping criterion (the change in the spread of

Pareto solutions is less than function tolerance) is satisfied. The optimization is converged after 100 iterations and optimum values of B, n, C and m values are obtained. The GA optimization process first uses all the data at different strain rates to minimize the objective function for B, n, C and after getting best suited C value, the next objective function considering the temperature effect the optimization is done. Table 9 shows the parameters of J-C model before and after the optimization.

It is observed that there is considerable improvement in predicting the values of J-C constants using the GA. The AARE percentage is far better for optimization process than that of the traditional curve fitting method. In section 5.2.1, it has been described that the effect of temperature is more pronounced in plastic region than that of the strain rate.

Table 9: The J-C parameters determined by curve fitting and GA method with prediction error of flow stress.

	B	n	C	m	AARE for $\dot{\varepsilon}$	AARE for T
Curve fitting	1978	1.005	0.027	0.64	6.71%	14.98%
Optimization	1860.5	1.0208	0.0067	0.87	4.81%	4.89%

The strain rate parameter C is slightly changed from 0.027 to 0.0067 but the temperature parameter has significant shift from 0.64 to 0.87 after optimization. Correspondingly, the AARE is minimized from 6.71% to 4.81% for different strain rates and from 14.98% to 4.89% for various temperature conditions. The differences between the constant parameters may be small but this small error can cause wrong estimation of flow stress which leads to the inaccurate prediction of material behavior.

To verify the calibrated parameters, the flow stresses are calculated by using Eq. (10) and the constants from the Table 9 for each fitting and optimization methods. The predicted results are compared with experimental stresses (measured stresses) by estimating the R^2 values for each test case shown in Table 10. A value of R^2 equals to 0.94 and 0.95,

respectively, at lower temperature (150℃) and lower strain rate (10^{-3}) by fitting method show fair accuracy for predicting stresses. However, it is further improved to 0.99 for each test conditions by optimization method. At higher temperature (450℃) and higer strain rate (10^{-1}), R^2 values of 0.22 and 0.52, respectively, are obtained which show lower performance of the J-C model with constants obtained by fitting methods. While the R^2 values of 0.87 and 0.76 obtained through optimization under the same test conditions indicate better options for the J-C model's ability to forecast material strength.

Table 10: Standard statistical measurements at different deforming conditions.

Temperature	R^2 (fitting)	R^2 (optimized)	Strain rate	R^2 (fitting)	R^2 (optimized)
150℃	0.94	0.99	10^{-3}	0.95	0.99
300℃	0.72	0.97	10^{-2}	0.87	0.95
450℃	0.22	0.87	10^{-1}	0.52	0.76

5.3 FE simulation results

For flat tensile model, simulation has been done at room temperature with cross-head speed of 9.6 mm/min to predict high strain rate (10^{-2} s^{-1}) behavior. On the other hand, for round tensile model, a predefined temperature field of 300℃ has been selected with cross-head speed of 4.3 mm/min for strain rate of 4.4×10^{-3} s^{-1}. Since the evaluated optimized parameters of J-C model predict more close material deformation behavior than the fitting parameters, these parameters are utilized in defining the material properties during the FE modelling.

Simulated and the experimental stress-strain curves are illustrated in Figs. 29a and 30a and the stress distribution patterns during simulation are shown in Figs. 29b and 30b. The yield and ultimate stress values in the experimental tensile test at the strain rate of 10^{-2} s^{-1} are 451

MPa and 1173 MPa, respectively, while, in the simulation, the yield and ultimate stress values are estimated as 430 MPa and 1199 MPa. There is 4.6 % deviation of the simulated yield stress value with respect to the experimental value and the simulation value is in the lower side. However, there is slightly over prediction in the simulated maximum stress value as observed. While rest of the stress values are between these deviation bounds and therefore it ascertains the J-C plastic behavior in high strain rate condition.

At elevated temperature tensile test, experimental yield strength value is 308 MPa and the maximum stress value is found to be 1194 MPa. The simulation results show the yield strength value of 294 MPa and maximum stress value of 1090 MPa. Simulation under predicts the stress value with 4.5% deviation in yield strength and 8.7% deviation in maximum stress value. From the experimental test data, it can be observed that the strain hardening behavior is linear up to 50% deformation and after that there is increase in hardening behavior. This can be explained by the ease of dislocation movement due to thermal energy but as the dislocation density increase with strain level, the pile up dislocation restrict the other dislocation movement. As the constitutive model included in the FE simulation does not consider all the microstructural changes like dislocation density, twinning, phase transformation etc. except varying strain rate and temperature condition, the above deviation might have occurred. However, it appears that the deviation reported above is within the permissible limit in computational simulation.

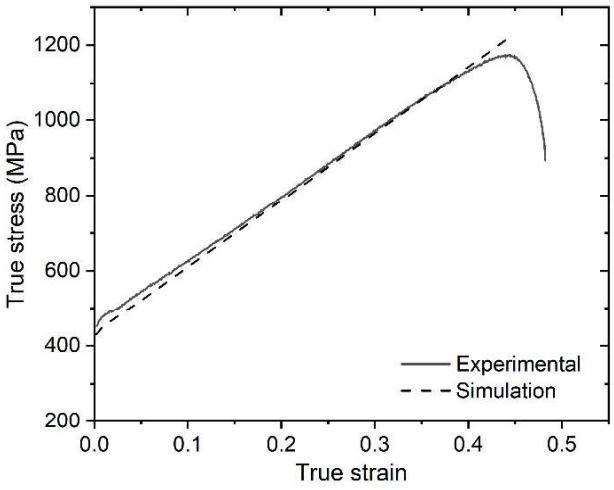

(a)

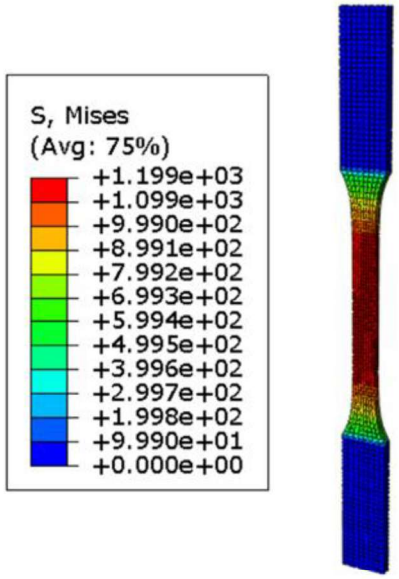

(b)

Fig. 29: (a) Tensile stress-strain curves in experiment and simulation at room temperature with strain rate of 10^{-2} s^{-1}, (b) stress distribution pattern in simulation.

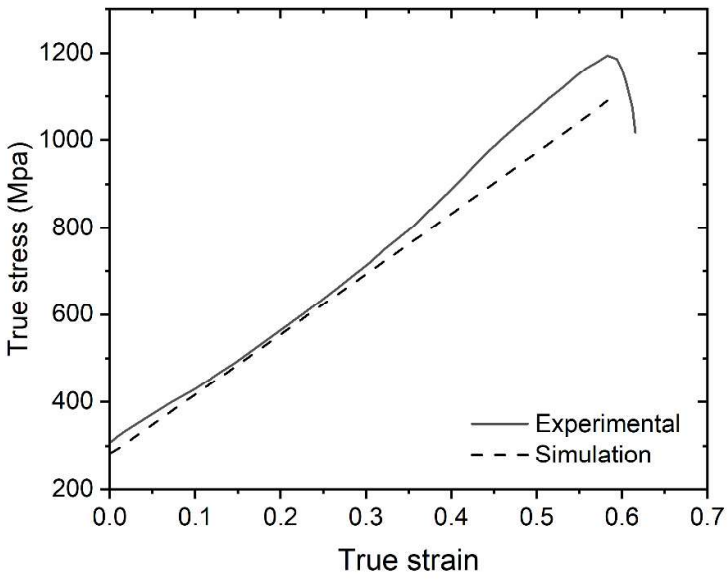

(a)

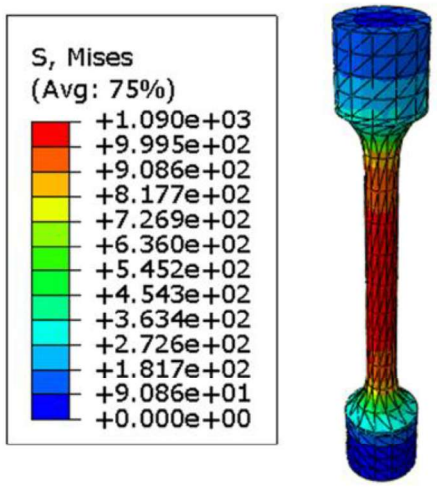

(b)

Fig. 30: (a) Tensile stress-strain curves in experiment and simulation at 300℃ with strain rate of 10^{-3} s^{-1}, (b) stress distribution pattern in simulation.

5.4 Conclusions

In this chapter, the tensile tests of the SS1 steel at different strain rates (10^{-4}, 10^{-3}, 10^{-2} and 10^{-1} s^{-1}) and at elevated temperatures (150°C, 300°C and 450°C) have been carried out to compute the J-C material model parameters. The present study permits us to list the following significant conclusions.

- The yield strength increases slightly with the increase in the strain rate due to positive strain rate sensitivity while the ultimate tensile strength remains almost same. At elevated temperature, the yield strength and ultimate strength drop due to thermal softening. Moreover, the ductility slightly differs with temperature except at 300 °C where 95% elongation is observed.
- The J–C model constants are initially evaluated by fitting method, and then, GA-based optimization technique has been used to obtain optimum values of J-C model constants. The optimized J-C model constants appear to be closer to reality as compared to the curve fitted J-C model constants.
- The strength of predictability of the model is investigated by comparing the predicted stress data with experimental stress data in terms of R^2 and AARE. It has been observed that after optimization the error is significantly reduced.
- FE simulation of the tensile test for SS1 steel has been conducted at moderate strain rate and temperature by implementing the calibrated J-C model constants in ABAQUS software. The simulation results are very close to the experimental data.
- The estimated error between the experimental and simulation data ensures that the proposed constitutive model may be suitable to study the deformation behaviour of SS1 at further elevated temperatures and higher strain rates.